Dalton Transactions

PAPER

View Article Online
View Journal | View Issue

Cite this: *Dalton Trans.*, 2017, **46**, 14256

Dinuclear nitrido-bridged ruthenium complexes bearing diimine ligands†

Julie Urgiles, Sarah R. Nathan, Samantha N. MacMillan and Justin J. Wilson *

Received 19th August 2017,
Accepted 2nd October 2017

DOI: 10.1039/c7dt03085a

rsc.li/dalton

Reactions of $K_3[Ru_2NCl_8(H_2O)_2]$ with 2,2′-bipyridine (bpy), 4,4′-dimethyl-2,2′-bipyridine (dmbpy), and 4,4′-dimethoxy-2,2′-bipyridine (dmobpy) yielded the nitrido-bridged dinuclear complexes $[Ru_2N(L)_2Cl_5(DMF)]$ where L = bpy (**1**), dmbpy (**2**), and dmobpy (**3**). The crystal structures of these complexes reveal a linear Ru–N–Ru moiety with each ruthenium center bearing a bidentate diimine ligand. The complexes were further characterized by NMR, IR, and UV-vis spectroscopic methods and cyclic voltammetry. Because the compounds bear some structural similarities with the mitochondrial calcium uptake inhibitor Ru360, the ability of these complexes to act in this capacity was evaluated. The results demonstrate that **1–3** all fail to block mitochondrial calcium uptake, revealing new facets of the structure–activity relationships for ruthenium-based mitochondrial calcium uptake inhibitors.

The linear Ru–O–Ru structural motif is observed in a wide range of functional complexes including water oxidation catalysts[1–3] and mitochondrial calcium uptake inhibitors.[4–8] A similar albeit less common motif is the linear bridging nitrido core, Ru–N–Ru, which is found in a smaller subset of compounds.[9–23] The significance of the μ-N^{3-} ligand, in comparison to μ-O^{2-}, in modulating the electronic and structural properties of these complexes remains an interesting fundamental question regarding their inorganic chemistry. To better understand the electronic structure of Ru–N–Ru compounds and to evaluate the relevance of the Ru–O–Ru core in the diverse activities of these compounds, the development of general synthetic methods to access nitrido-bridged derivatives is relevant. With respect to synthetic methods to access related oxo-bridged complexes, we have previously shown that the $[Ru_2OCl_{10}]^{4-}$ anion (Chart 1) undergoes ligand substitution reactions at the axial and equatorial sites with the Ru–O–Ru core remaining intact.[7] To access new nitrido-bridged compounds, we explored the ligand substitution chemistry of the analogous μ-nitrido anion[9,24–26] $[Ru_2NCl_8(H_2O)_2]^{3-}$ (Chart 1) to demonstrate its suitability as an appropriate synthon for novel Ru–N–Ru complexes. Specifically, we explored the reactivity of this compound with 2,2′-bipyridine and two other derivatives to generate three new dinuclear nitrido-bridged ruthenium complexes bearing diimine ligands.

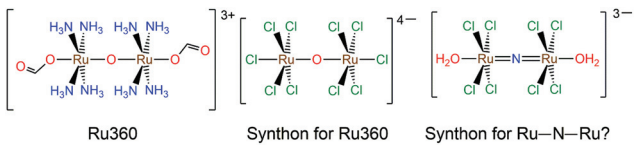

Chart 1 Structures of the MCU inhibitor Ru360, $[Ru_2OCl_{10}]^{4-}$, and $[Ru_2NCl_8(H_2O)_2]^{3-}$.

Although the fundamental properties of such complexes are of interest, our synthetic efforts stemmed from our research program to develop novel ruthenium-based mitochondrial calcium uptake inhibitors.[7,8] The ability to modulate mitochondrial calcium uptake is of significance because the flux of calcium ions in and out of the mitochondria triggers a wide range of cellular processes that are critical for normal physiological function.[27] Excessive mitochondrial calcium levels induce pathological cell death. *In vivo*, mitochondrial calcium overload may arise as a consequence of ischemic reperfusion injury, a condition where cells undergo a rapid transition from hypoxia to normoxia.[28,29] Inhibition of mitochondrial calcium uptake in these cases may lead to beneficial therapeutic effects for the prevention of reperfusion injury.[30–32] Thus, the investigation of inhibitors of the mitochondrial transport protein, the mitochondrial calcium uniporter (MCU),[33] is of potential value for the development of new drug candidates for reperfusion injury.[34]

The best-characterized inhibitor of the MCU is the dinuclear oxo-bridged ruthenium complex Ru360 $[(HCO_2)(NH_3)_4Ru(\mu\text{-}O)Ru(NH_3)_4(O_2CH)]^{3+}$ (Chart 1).[4–6] The mechanism by which this compound inhibits the MCU, however, is not understood, and therefore the structural fea-

Department of Chemistry and Chemical Biology, Cornell University, Ithaca, New York 14853, USA. E-mail: jjw275@cornell.edu

†Electronic supplementary information (ESI) available: Experimental procedures, characterization data, X-ray crystallographic data. CCDC 1569567 and 1569568. For ESI and crystallographic data in CIF or other electronic format see DOI: 10.1039/c7dt03085a

tures that give rise to its MCU-inhibitory properties are unknown. We hypothesized that the dinuclear ruthenium complexes with bridging nitrido ligands and diimine supporting ligands studied in this investigation may be new members of this class of compounds. Our studies, however, revealed that these compounds are not inhibitors of the MCU. This result sheds light on the structure–activity relationships of ruthenium-based MCU inhibitors.

Experimental

Materials and methods

Commercially available ruthenium trichloride hydrate ($RuCl_3{\cdot}nH_2O$, 40% Ru) was used to prepare $K_3[Ru_2NCl_8(H_2O)_2]$ following a modification of the published procedure.[10] The ligand 2,2′-bipyridine (bpy) was obtained from Alfa Aesar, whereas 4,4′-dimethoxy-2,2′-bipyridine (dmobpy) and 4,4′-dimethyl-2,2′-bipyridine (dmbpy) were purchased from Sigma-Aldrich. These reagents were used as received. Solvents used were of ACS grade or higher.

Physical measurements

^{1}H NMR spectra were acquired on a 600 MHz INOVA spectrometer. $^{13}C\{^1H\}$ NMR spectra were acquired on a 500 MHz Bruker AV 3HD spectrometer equipped with a broadband Prodigy cryoprobe. IR spectra were obtained using a Bruker Hyperion ATIR with ZnSe ATR attachment for solid powders. UV-vis samples were prepared in dimethyl sulfoxide (DMSO), and an Agilent Cary 8454 UV-visible spectrophotometer was used to acquire spectra. A Pine Instruments WaveNow potentiostat and a three electrode cell comprising a glassy carbon working electrode, a platinum counter electrode, and a silver reference electrode were used to acquire cyclic voltammograms at a scan rate of 100 mV s^{-1}. Compounds were dissolved in a 0.10 M solution of $[Bu_4N][PF_6]$ in *N*,*N*-dimethylformamide (DMF) that was dried over molecular sieves (4 Å). Nitrogen gas was bubbled into the solution to deoxygenate the cell before analysis. An internal standard, ferrocene, $E_{1/2}$ = 0.45 V *vs.* saturated calomel electrode (SCE), was used to reference the potentials.[35,36] Elemental analyses (CHN) were performed by Atlantic Microlab Inc., Norcross, Georgia, USA.

Synthesis of $[Ru_2N(bpy)_2Cl_5(DMF)]{\cdot}0.5H_2O$ (1·0.5H_2O)

Suspensions of $K_3[Ru_2NCl_8(H_2O)_2]$ (300 mg, 0.459 mmol) and 2,2′-bipyridine (358 mg, 2.295 mmol) in 3 mL of water and 7 mL of acetone, respectively, were warmed at 45 °C for 10 min to ensure full dissolution of these compounds. Once dissolved, the resulting solutions were mixed and heated under reflux for 8 h. The resulting red-brown crude solid was isolated by filtration and washed with acetone and diethyl ether. This crude solid (180 mg) was suspended in DMF (12 mL), sonicated for 15 min, stirred at rt for 30 min, and then filtered. The vapor diffusion of methanol into the resulting dark red filtrate afforded red crystals of the desired compound after a week. Yield: 60 mg, 17%. ^{1}H NMR (600 MHz, DMSO-d_6): δ 9.98 (dd, J = 5.6 and 1.5 Hz, 1H), 9.61 (dd, J = 5.7 and 1.5 Hz, 2H), 8.85 (dd, J = 5.6 and 1.7 Hz, 1H), 8.71 (d, J = 8.0 Hz, 2H), 8.61 (d, J = 8.1 Hz, 1H), 8.53 (d, J = 8.2 Hz, 1H), 8.39 (td, J = 7.8 and 1.5 Hz, 2H), 8.20 (td, J = 7.9 and 1.5 Hz, 1H), 8.16 (td, J = 7.8 and 1.7 Hz, 1H), 7.84 (ddd, J = 7.8, 5.6, and 1.3 Hz, 2H), 7.75 (ddd, J = 7.8, 5.6, and 1.3 Hz, 1H), 7.61 (ddd, J = 7.8, 5.5 and 1.0 Hz, 1H). $^{13}C\{^1H\}$ NMR (125 MHz, DMSO-d_6): δ 158.18, 155.45, 154.74, 153.33, 152.71, 149.20, 140.94, 140.14, 139.38, 126.09, 126.02, 125.76, 123.56, 123.27, 122.55. IR (ATR, cm^{-1}): 1638 s, 1601 w, 1443 w, 1422 w, 1369 w, 1030 s, 1074 w, 766 vs, 727 s, and 692 s. Anal. calcd % for **1**·0.5H_2O, $C_{23}H_{24}Cl_5N_6O_{1.5}Ru_2$: C, 35.06; H, 3.07; N, 10.67. Found: C, 35.27; H, 3.50; N, 10.53.

Synthesis of $[Ru_2N(dmbpy)_2Cl_5(DMF)]{\cdot}2H_2O$ (2·2H_2O)

Suspensions of $K_3[Ru_2NCl_8(H_2O)_2]$ (300 mg, 0.459 mmol) and 4,4′-dimethyl-2,2′-bipyridine (338 mg, 1.836 mmol) in 3 mL of water and 7 mL of acetone, respectively, were warmed at 45 °C for 10 min. The resulting acetone suspension and aqueous solution were mixed and heated under reflux for 6 h. The resulting red-brown crude solid was isolated by filtration and washed with chloroform and diethyl ether. To further purify the complex from excess dmbpy ligand, the crude solid was suspended in 10 mL of chloroform and heated under reflux for 2 h, and then isolated again by filtration while still warm. As a final means of purification, the solid (120 mg) was suspended in 6 mL of DMF, sonicated for 30 min, stirred at rt for 1 h, and then filtered. The dark red filtrate, which contains pure product, was subjected to vapor diffusion with methanol. Over the course of the week, red crystals of the desired product were obtained. Yield: 14 mg (3.5%). Note: additional batches of pure product can be obtained by repeating the sonication procedure with the crude solid. The product is only sparingly soluble in DMF, so the isolation of more compound requires repeated extractions in this solvent. ^{1}H NMR (600 MHz, DMSO-d_6): δ 9.77 (d, J = 5.8 Hz, 1H), 9.40 (d, J = 5.6 Hz, 2H), 8.67 (d, J = 5.7 Hz, 1H), 8.55 (s, 2H), 8.45 (s, 1H), 8.37 (s, 1H), 7.65 (d, J = 6.0 Hz, 2H), 7.56 (d, J = 5.9 Hz, 1H), 7.42 (d, J = 5.9 Hz, 1H), 2.60 (s, 2H), 2.59 (s, 1H), 2.45 (s, 1H). $^{13}C\{^1H\}$ NMR (125 MHz, DMSO-d_6): δ 157.67, 154.67, 154.24, 153.10, 152.48, 151.84, 151.76, 150.99, 148.45, 126.70, 126.38, 126.18, 123.97, 123.66, 122.94, 21.00, 20.80, 20.43. IR (ATR, cm^{-1}): 1638 s, 1616 vs, 1435 w, 1366 w, 1020 w, 1032 s, 1065 s, 1084 w, 831 s, and 690 w. Anal. calcd % for **2**·2H_2O, $C_{27}H_{35}Cl_5N_6O_3Ru_2$: C, 37.23; H, 4.05; N, 9.65. Found: C, 37.27; H, 4.17; N 9.60.

Synthesis of $[Ru_2N(dmobpy)_2Cl_5(DMF)]$ (3)

Suspensions of $K_3[Ru_2NCl_8(H_2O)_2]$ (300 mg, 0.459 mmol) and 4,4′-dimethoxy-2,2′-bipyridine (397 mg, 1.836 mmol) in 3 mL of water and 7 mL of acetone, respectively, were warmed at 45 °C for 10 min. The resulting acetone suspension and aqueous solution were mixed and heated under reflux for 6 h. The resulting red-brown crude solid was isolated by filtration and washed with chloroform and diethyl ether. To remove excess dmobpy ligand, the crude solid was suspended in 10 mL of chloroform and heated under reflux for 2 h, and then

isolated again by filtration. For further purification, the solid was then suspended in 10 mL of 6 : 4 acetone : water, heated at reflux for 4 h, and then filtered. This crude solid (120 mg) was suspended in 12 mL of DMF, sonicated for 30 min, stirred at rt for 1 h, and then filtered. The dark red filtrate, which contains pure product, was subjected to vapor diffusion with methanol to afford the product as red crystals. Yield: 22 mg (5.3%). Note: more pure product can be obtained by sequential extractions of the remaining crude solid with DMF as described above for compound **2**. ^{1}H NMR (600 MHz, DMSO-d_6): δ 9.71 (d, J = 6.6 Hz, 1H), 9.35 (d, J = 6.7 Hz, 2H), 8.66 (d, J = 6.5 Hz, 1H), 8.29 (d, J = 2.8 Hz, 2H), 8.22 (d, J = 2.8 Hz, 1H), 8.10 (d, J = 2.5 Hz, 1H), 7.42 (dd, J = 6.7 and 2.7 Hz, 2H), 7.34 (dd, J = 6.7 and 2.7 Hz, 1H), 7.21 (dd, J = 6.6 and 2.5 Hz, 1H), 4.08 (s, 2H), 4.07 (s, 1H), 3.97 (s, 1H). ^{13}C{^{1}H} NMR (125 MHz, DMSO-d_6): δ 168.29, 167.90, 167.70, 159.35, 156.27, 155.67, 155.00, 153.61, 150.21, 111.65, 111.19, 110.80, 109.83, 108.90, 57.00, 56.87, 56.71. IR (ATR, cm^{-1}): 1609 vs, 1559 w, 1495 w, 1418 w, 1341 w, 1279 w, 1229 s, 1015 s, 1030 vs, 1049 vs, 1063 s, 1074 vw, 866 w, and 835 s. Anal. calcd % for **3**, $C_{27}H_{31}Cl_5N_6O_5Ru_2$: C, 36.07; H, 3.48; N, 9.35. Found: C, 35.80; H, 3.64; N, 9.15.

X-ray crystallography

Low-temperature X-ray diffraction data for **1** and **3** were collected on a Rigaku XtaLAB Synergy diffractometer coupled to a Rigaku Hypix detector with Mo Kα radiation (λ = 0.71073 Å) and Cu Kα radiation (λ = 1.54184 Å), respectively, from PhotonJet micro-focus X-ray sources at 100 K. The diffraction images were processed and scaled using the CrysAlisPro software.[37] The structures were solved through intrinsic phasing using SHELXT[38] and refined against F^2 on all data by full-matrix least squares with SHELXL[39] following established refinement strategies.[40] All non-hydrogen atoms were refined anisotropically. All hydrogen atoms bound to carbon were included in the model at geometrically calculated positions and refined using a riding model. The isotropic displacement parameters of all hydrogen atoms were fixed to 1.2 times the U_{eq} value of the atoms they are linked to (1.5 times for methyl groups). The unit cell of **1** contains 3 methanol molecules and the unit cell of **3** contains 3 DMF molecules, which have been treated as diffuse contributions to the overall scattering without specific atom positions using the solvent mask routine in Olex2.[41] Details of the data quality and a summary of the residual values of the refinements are listed in Table 1. Crystallographic data in the form of cif files have been deposited in the Cambridge Crystallographic Data Centre under the accession numbers CCDC 1569567 and 1569568 for **1** and **3**, respectively.†

Table 1 X-ray crystallographic data collection and refinement parameters for **1** and **3**

	1	**3**
Formula	$C_{23}H_{23}Cl_5N_6ORu_2$	$C_{27}H_{31}Cl_5N_6O_5Ru_2$
fw	778.86	898.97
Space group	$P\bar{1}$	$P\bar{1}$
a, Å	9.79250(10)	12.2823(3)
b, Å	11.28330(10)	12.5160(2)
c, Å	15.4471(2)	15.2094(2)
α, °	77.1190(10)	98.4980(10)
β, °	84.0320(10)	106.815(2)
γ, °	71.1160(10)	111.247(2)
V, Å^3	1573.34(3)	2000.61(7)
Z	2	2
ρ_{calcd}, g cm^{-3}	1.644	1.492
T, K	100.00(10)	100.01(10)
λ, Å	0.71073	1.54184
μ(Mo Kα), mm^{-1}	1.411	
μ(Cu Kα), mm^{-1}		9.518
Θ range, °	1.947 to 25.681	3.165 to 70.072
Completeness to Θ (%)	100.0	99.8
Total no. of data	37 538	27 775
No. of unique data	5961	7570
No. of parameters	336	412
R_1 [a]	0.0170	0.0257
wR_2 [b]	0.0407	0.0698
GOF [c]	1.015	1.075
Max, min peaks, e Å^{-3}	0.393, −0.351	0.626, −0.797

[a] $R_1 = \sum||F_o| - |F_c||/\sum|F_o|$ for $I > 2\sigma$. [b] w$R_2 = \{\sum[w(F_o^2 - F_c^2)^2]/\sum[w(F_o^2)^2]\}^{1/2}$ for $I > 2\sigma$. [c] GoF $= \{\sum[w(F_o^2 - F_c^2)^2]/(n-p)\}^{1/2}$, where n is the number of data and p is the number of refined parameters.

Cell culture

HeLa (human cervical cancer) cells were grown as adherent monolayers in growth medium consisting of Dulbecco's Modified Eagle's Medium (DMEM) supplemented with 10% fetal bovine serum (FBS). The cultures were grown in 100 cm^2 petri dishes in an incubator at 37 °C with a humidified atmosphere composed of 5% CO_2. Cells were tested for mycoplasma contamination at least monthly with the PlasmoTest™ Mycoplasma Detection Kit (InvivoGen).

Cell viability assays

Stock solutions of the complexes were prepared in DMSO at concentrations between 2–3 mM. Cells were seeded in a 96-well plate at a density of 2000 cells per well. After 24 h, the growth medium was removed and replaced with 200 μL of growth medium containing varied concentrations of the complexes of interest. After an additional 72 h incubation, the medium was removed and replaced with 200 μL of 5 mg mL^{-1} 3-(4,5-dimethylthiazol-2-yl)-2,5-diphenyltetrazolium bromide (MTT), diluted to 1 mg mL^{-1} in serum-free medium. After 4–6 h, the MTT was removed, and the resulting purple formazan crystals were dissolved in 200 μL DMSO containing 17% 0.1 M glycine and 0.1 M NaCl at pH 10.5. The absorbance at 570 nm in each well was determined using a BioTek Synergy HT plate reader. Six replicates per concentration level and at least three independent experiments were completed for each compound.

Mitochondrial calcium uptake in permeabilized HeLa cells

HeLa (human cervical cancer) cells were amplified in 500 cm^2 petri dishes. Following a previously reported procedure,[7,42] growth media was removed, and HeLa cells at 80–100% confluency were washed once with 1× PBS, incubated with 1 mM EDTA in 1× PBS for 10 min, and gently agitated to detach cells from the surface. Cells were centrifuged for 10 minutes at

1000× (5310*g*) and resuspended in a pH 7.4 buffered glucose-containing salt solution (BGSS: 110 mM KCl, 1 mM KH_2PO_4, 1 mM $MgCl_2$, 20 mM HEPES, 5 mM sodium succinate, 30 μM EGTA, 1 mg mL^{-1} glucose) with a final cell density of 3.25 × 10^6 cells per mL. To permeabilize and track calcium uptake in the cells, the suspension was stirred in a 1 cm pathlength acrylic cuvette at 37 °C with 40 μM digitonin (diluted from a DMSO stock solution) and 2 μM of Calcium Green-5N (Invitrogen, aqueous solution). A SLM 8100C steady-state fluorimeter (excitation = 506 nm, emission = 532 nm) was used to monitor the fluorescence of the Calcium Green-5N dye. $CaCl_2$ was added in boluses of 7.5 μM to test for mitochondrial calcium uptake inhibition. After two calcium boluses were added to the solution to verify cellular action and achieve a stable emission intensity baseline, compound **1** was added (5 μM, diluted from DMSO). The experiment was repeated with cell solutions using compounds **2** and **3** to test for their possible mitochondrial calcium uptake inhibitory properties.

Results and discussion

Synthesis and characterization

As part of our research group's efforts to develop new inhibitors of the MCU,[7,8] we explored the chemistry of the complex $K_3[Ru_2NCl_8(H_2O)_2]$ to evaluate its potential as a starting material for new diruthenium μ-nitrido complexes that are structural analogues of Ru360. To synthesize $K_3[Ru_2NCl_8(H_2O)_2]$, a previously reported procedure was used (Scheme 1).[10] Briefly, $RuCl_3{\cdot}nH_2O$ was first converted to $K_2[RuCl_5NO]$ by the reaction of this salt with KNO_2 and KCl in HCl. Reduction of the nitrosyl with $SnCl_2$ in HCl afforded the desired μ-nitrido complex $K_3[Ru_2NCl_8(H_2O)_2]$. The lability of the chloride ligands of this complex to ligand substitution reactions has previously been demonstrated.[10,11] Notably, the substitution reaction of this complex with ethylenediamine afforded the homoleptic complex $[Ru_2N(en)_5]^{5+}$, which was characterized conclusively by X-ray crystallography and NMR spectroscopy.[12] By contrast, other products of the substitution reactions of $K_3[Ru_2NCl_8(H_2O)_2]$ were characterized only by IR spectroscopy and elemental analysis, giving rise to some ambiguity in their structure and identity.[10,11] We sought to reinvestigate this chemistry to more conclusively characterize the resulting products and probe the ligand substitution reactivity of this compound. In accordance with the literature method for the synthesis of $[Ru_2N(bpy)_4Cl_2]^{3+}$,[11] we initially heated an acetone–water mixture solution containing $K_3[Ru_2NCl_8(H_2O)_2]$ to reflux in the presence of either 2,2′-bipyridine (bpy), 4,4′-dimethyl-2,2′-bipyridine (dmbpy), or 4,4′-dimethoxy-2,2′-bipyridine (dmobpy). Upon recrystallization of the crude products from DMF, red crystals of compounds **1–3** $[Ru_2N(NN)_2Cl_5(DMF)]$ where NN = bpy (**1**), dmbpy (**2**), or dmobpy (**3**) were isolated in yields ranging from 3–16% (Scheme 1). Although we did not fully optimize the reaction conditions for these products, the remaining insoluble crude material can be further extracted with DMF and recrystallized by MeOH vapor diffusion to obtain additional crops of **1–3**.

The previously reported reaction of $K_3[Ru_2NCl_8(H_2O)_2]$ with bpy reportedly afforded the cation $[Ru_2N(bpy)_4Cl_2]^{3+}$, which was characterized only by IR spectroscopy and elemental analysis.[11] Related nitrido-bridged dinuclear ruthenium complexes bearing bpy ligands, $[Ru_2N(bpy)_2Cl_5(H_2O)]$ and $(H_5O_2)[Ru_2N(bpy)_2Cl_6]$ were isolated from the high temperature reaction of $[Ru(bpy)(CO)_2Cl_2]$ in HCl–HNO_3 mixtures and were structurally characterized by X-ray crystallography.[14] These structures both show a single bpy ligand coordinated in a bidentate manner to each ruthenium center. The orientation of the bpy ligands in these complexes are such that both nitrogen donor atoms reside on the equatorial plane, in the *cis* disposition relative to the bridging nitrido ligand. Although the ^{1}H NMR spectra of these complexes was not reported, symmetric spectra would be expected given the chemical equivalence of the two bpy ligands. By contrast, the ^{1}H NMR spectrum of our synthesized compounds **1–3** revealed three distinct sets of aromatic spin systems in a ratio of 2 : 1 : 1 (Fig. 1 and S1–S6†), indicating that we had isolated a less symmetric compound than the previously reported $[Ru_2N(bpy)_2Cl_5(H_2O)]$, $(H_5O_2)[Ru_2N(bpy)_2Cl_6]$, and $[Ru_2N(bpy)_4Cl_2]^{3+}$ complexes. Of note, in the aliphatic region of the ^{1}H NMR spectrum, resonances arising from one equiv. of free DMF at 7.95, 2.89, and 2.73 ppm are present. The observation of free DMF suggests that

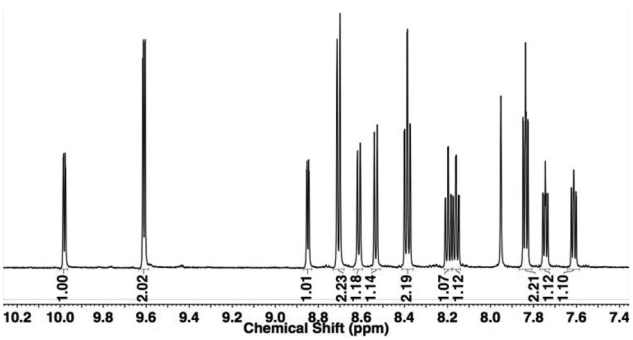

Fig. 1 ^{1}H NMR spectrum of **1** in DMSO-d_6.

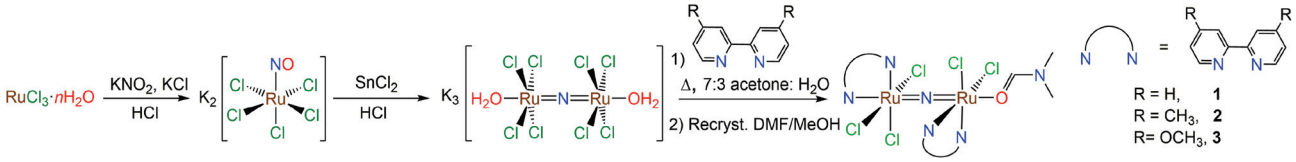

Scheme 1 Synthesis of compounds **1–3**.

the axial DMF ligand is labile and is displaced by the DMSO solvent. Upon further incubation of the complex in DMSO-d_6, no changes in the NMR spectra are observed. This result suggests that the chloride ligands are stable to solvolysis, as the sequential displacement of these ligands by DMSO would give rise to a complicated superposition of NMR resonances arising from a combination of asymmetric solvated products.

X-ray crystallography

Single-crystals of **1** and **3** were grown from DMF solutions and analysed by X-ray diffraction. Suitable crystals of **2** for X-ray diffraction could not be obtained. The crystal structures of **1** and **3** conclusively reveal them to be $[Ru_2N(bpy)_2Cl_5(DMF)]$ and $[Ru_2N(dmobpy)_2Cl_5(DMF)]$ (Fig. 2). The linear Ru–N–Ru moiety is present, demonstrating the value of $K_3[Ru_2NCl_8(H_2O)_2]$ as a synthon for compounds bearing this structural feature. The complex is asymmetric; one ruthenium possesses an octahedral coordination geometry fulfilled by a diimine ligand, three chlorides, and the bridging nitrido, and the other octahedral ruthenium center is coordinated by a diimine ligand, two chlorides, a DMF solvent molecule, and the bridging nitrido.

Notably, the orientations of the diimine ligands differ from the previously reported complexes (Chart 2); in complexes **1–3**, one diimine resides with both nitrogen donors occupying equatorial binding sites, and the second diimine occupies both an axial position, trans to the bridging nitrido, and an equatorial position. For the previously reported $[Ru_2N(bpy)_2Cl_5(H_2O)]$,[14] both bpy ligands assume equatorial positions on the two ruthenium centers. The configuration of the diimine ligands in **1–3** is consistent with their ^{1}H NMR spectra, as the axial/equatorial diimine ligands will give rise to two distinct aromatic spin systems and the equatorial/equatorial diimine ligand will yield a single spin system. Furthermore, this structure is inconsistent with the previously reported complex $[Ru_2N(bpy)_4Cl_2]^{3+}$, the purported reaction product of $K_3[Ru_2NCl_8(H_2O)_2]$ with bpy.[11]

Relevant interatomic distances and angles for **1** and **3** are collected in Table 2. The Ru–N nitrido distances are symmetric and range from 1.7219(18) to 1.7375(18) Å. No significant deviations in these distances between the two compounds are noted, and the distances are similar to those found in previously reported dinuclear nitrido-bridged complexes.[12,14,15] The Ru–N–Ru angles, which deviate slightly from 180°, are 173.10(9)° and 177.27(11)° for **1** and **3**, respectively. The equatorial and axial Ru–ligand interatomic distances are disparate. For example, the axial Ru–N2 distance (2.1626(14) and 2.1546(19) Å for **1** and **3**, respectively) is approximately 0.1 Å longer than the corresponding equatorial Ru–N distances, which are between 2.0532(14) and 2.0646(18) Å. The elongation of the axial bond distances is most likely a consequence of the strong trans influence of the bridging nitrido ligand.

Infrared and UV-visible spectroscopy

The IR and UV-vis spectroscopic properties of **1–3** were also investigated. A diagnostic feature in nitrido-bridged ruthenium complexes is the asymmetric Ru–N–Ru stretching mode. This transition ranges from 1070 to 1080 cm^{-1} for the starting anion $[Ru_2NCl_8(H_2O)_2]^{3-}$ in a manner that depends on the nature of counterion.[43] The conclusive identification of this mode in the IR spectrum of **1–3**, however, was challenged by the presence of ligand vibrational features within this region (Fig. S7–S9†). Absorbance bands at 1030 and 1074 cm^{-1}, 1032 and 1065 cm^{-1}, and 1030 and 1063 cm^{-1}, are tentatively assigned as the symmetric and asymmetric Ru–N–Ru stretching frequencies in **1–3**. These values are consistent with those of the previously reported all-equatorial bpy complex, $[Ru_2N(bpy)_2Cl_5(H_2O)]$,[14] suggesting that the stereochemical

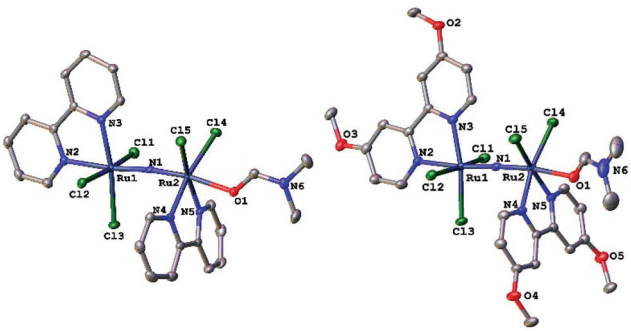

Fig. 2 X-ray crystal structure of **1** and **3**. Ellipsoids are draw at the 50% probability level. Hydrogen atoms are omitted for clarity.

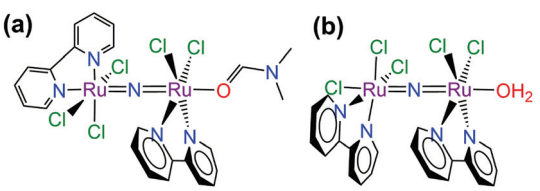

Chart 2 (a) Structure of **1** isolated in this work. (b) Structure of $[Ru_2N(bpy)_2Cl_5(H_2O)]$, characterized by Haukka, *et al.* (see ref. 14).

Table 2 Selected interatomic distances (Å) and angles (°) for **1** and **3**[a]

	1	3
Nitrido bridge parameters		
Ru2–N1–Ru1	173.10(9)	177.22(11)
Ru1–N1	1.7351(14)	1.7375(18)
Ru2–N1	1.7256(13)	1.7219(18)
Equatorial parameters		
Ru1–N3	2.0548(14)	2.0646(18)
Ru1–Cl1	2.3791(4)	2.3603(5)
Ru1–Cl2	2.3718(4)	2.3948(5)
Ru1–Cl3	2.3815(4)	2.3831(5)
Ru2–N4	2.0532(14)	2.0567(18)
Ru2–N5	2.0607(15)	2.0596(19)
Ru2–Cl4	2.3722(4)	2.3638(5)
Ru2–Cl5	2.3662(4)	2.3728(6)
Axial parameters		
Ru1–N2	2.1626(14)	2.1546(19)
Ru2–O1	2.1435(11)	2.1481(16)

[a] Atoms are labeled as shown in Fig. 2.

arrangement of these ligands have little effect on the ruthenium–nitrido bond.

The UV-vis spectra of the compounds in dimethyl sulfoxide (DMSO) (Fig. 3 and Table S1†) were characterized by low-energy transitions between 350 and 380 nm, and a higher energy transition near 300 nm. The low-energy transition is assigned as a metal-to-ligand charge transfer. The energy of this transition shifts noticeably as the substituents on the bpy ligands are altered through **1–3**. As more electron-donating groups are introduced, the MLCT energy shifts to higher energy. This result is consistent with the effect of electron donating groups, which increase the energy of the accepting ligand π^* orbital of the diimine ligand.[44]

Electrochemistry

The electrochemical properties of **1–3** were investigated by cyclic voltammetry (Fig. 4). Anodic scans reveal the presence of a quasi-reversible oxidation feature, which we tentatively attribute to the $Ru^{V}Ru^{IV}/Ru^{IV}Ru^{IV}$ couple. In related nitrido-bridged dinuclear complexes, the $Ru^{V}Ru^{IV}$ state could be accessed at relatively mild potentials, signifying the ability of the nitrido ligand to stabilize high oxidation states.[19,20,22] This quasi-reversible oxidation ($E_{1/2}$) to the $Ru^{V}Ru^{IV}$ state occurs at 1.33, 1.25, and 1.19 V *vs.* SCE for **1–3**, respectively, demonstrating that the donating methyl and methoxy groups on **2** and **3** stabilize the higher oxidation states. Upon scanning cathodically, an irreversible reduction feature is observed, which is tentatively assigned to the $Ru^{IV}Ru^{IV}/Ru^{IV}Ru^{III}$ couple. The peak potentials (E_p) of this irreversible reduction are −1.03, −1.10, and −1.22 V *vs.* SCE for **1–3**, respectively. As expected, these values indicate that reduction occurs at more positive potentials when the bpy ligand has less electron-donating substituents. Upon cycling back to anodic potentials, a new quasi-reversible oxidation feature, presumably arising from the irreversible reduction product, is observed. Notably, the $E_{1/2}$ of this quasi-reversible oxidation is relatively invariant for the three complexes at 0.95 V *vs.* SCE. This result suggests that this oxidation might arise from a ruthenium-containing product that lacks the diimine ligands.

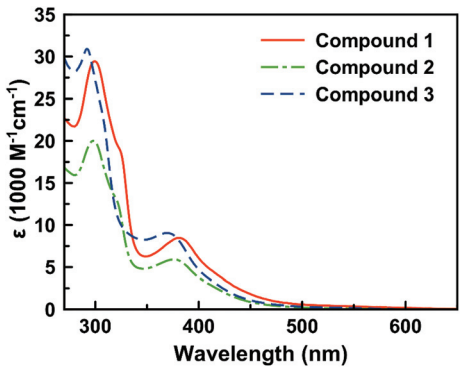

Fig. 3 UV-vis spectra of **1–3** in DMSO at room temperature (24–25 °C).

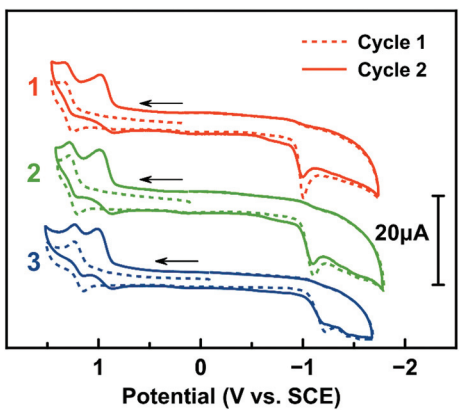

Fig. 4 Cyclic voltammograms of **1–3** in 0.10 M $[Bu_4N][PF_6]$ in DMF at room temperature (24–25 °C), using a scan rate of 100 mV s^{-1}.

Biological activity

Having established the structural and physical characterization of **1–3**, we sought to evaluate their potential as MCU inhibitors. Because the practical implementation of MCU inhibitors requires that they be non-toxic, we first determined the cytotoxicity of **1–3** against HeLa cells. The resulting dose–response curves for **1–3** are shown in Fig. 5. This data shows that these compounds are relatively non-toxic at the micromolar concentrations that would be used for MCU inhibition. The viability of the cells at the maximum 200 μM dose tested was >70% for all three complexes.

Given the low toxicity of these complexes, their mitochondrial calcium uptake inhibitory properties were further investigated, following a previously reported procedure.[42] HeLa cells were permeabilized with digitonin and suspended in a cuvette with the calcium sensor Calcium Green-5N. The emission response of this dye was monitored by fluorescence spectroscopy. In untreated cells, the addition of a 7.5 μM bolus of Ca^{2+} leads to an immediate increase in emission intensity as these ions bind the Calcium Green-5N. The intensity decays as these calcium ions are taken up by the mitochondria. When the cells are treated with the diaqua analogue of Ru360 $[(OH_2)(NH_3)_4Ru(\mu\text{-}O)Ru(NH_3)_4(OH_2)]^{5+}$,[7] a known mitochondrial calcium uptake inhibitor, the addition of a 7.5 μM Ca^{2+} bolus gives rise to an increase in emission intensity that

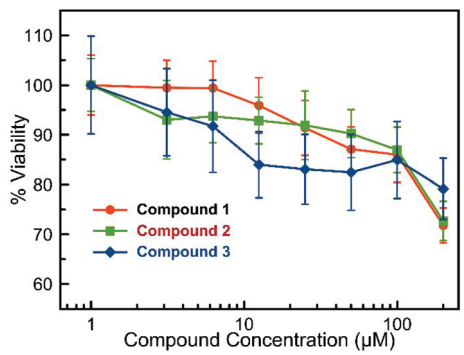

Fig. 5 Cytotoxicity of compounds **1–3** in HeLa cells.

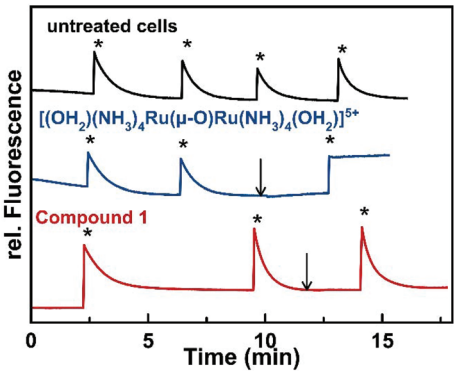

Fig. 6 Mitochondrial calcium uptake measurements in permeabilized HeLa cells in the absence (top) or presence of 5 μM $[(OH_2)(NH_3)_4Ru(\mu\text{-}O)Ru(NH_3)_4(OH_2)]^{3+}$ (middle) or **1** (bottom). The asterisk indicates when a bolus of Ca^{2+} ions (7.5 μM) was added. The arrows indicate when 5 μM of the ruthenium compound was added. The fluorescence was re-normalized after addition of the ruthenium compound.

remains constant because the calcium ions are not taken up by the mitochondria (Fig. 6). We carried out this experiment in the presence of either 5 μM **1**, **2**, or **3**. The addition of the Ca^{2+} bolus in the presence of these complexes gave rise to rapid increase and then steady decay in emission that was indistinguishable from the control cells. Therefore, none of these three compounds exhibit mitochondrial calcium uptake inhibitory properties (Fig. 6 and S10–S12†).

Conclusions

In summary, we have demonstrated that $K_3[Ru_2NCl_8(H_2O)_2]$ is a useful starting material to access compounds with the linear Ru–N–Ru motif *via* ligand substitution reactions. The reactions of this compound with bpy and its derivatives led to compounds **1–3**, which were fully characterized structurally and spectroscopically. The cytotoxicity and MCU-inhibitory properties of **1–3** were evaluated. These compounds were not cytotoxic and did not exhibit MCU inhibitory properties. The lack of MCU inhibitory activity is perhaps not surprising given the structural dissimilarity of these compounds in comparison to Ru360. For example, recent molecular mechanics studies of Ru360 docked in the pore channel of the MCU reveal critical hydrogen bonding interactions between the amino acid residues and ammine ligands of Ru360.[45] The lack of hydrogen bond donors in **1–3** may preclude their successful inhibition of the MCU. Additionally, unlike Ru360, **1–3** are charge-neutral. Electrostatic interactions may also be critical for the MCU inhibitory activity, providing another possible explanation for the failure of **1–3** in this capacity. Ongoing work is focused on exploring the reactivity of $K_3[Ru_2NCl_8(H_2O)_2]$ to access novel MCU inhibitors.

Conflicts of interest

There are no conflicts to declare.

Acknowledgements

This research was supported by Cornell University. S. R. N. thanks the NSF for a graduate fellowship (DGE-1650441). This work made use of instrumentation in the Cornell Center for Materials Research (CCMR) and the Cornell NMR Facility, which are supported by the NSF under grants CHE-1531632 and DMR-1120296, respectively. Drs Dave Holowka and Nikki A. Thiele are thanked for experimental assistance.

Notes and references

1 J. A. Baumann and T. J. Meyer, *Inorg. Chem.*, 1980, **19**, 345–350.
2 F. Liu, J. J. Concepcion, J. W. Jurss, T. Cardolaccia, J. L. Templeton and T. J. Meyer, *Inorg. Chem.*, 2008, **47**, 1727–1752.
3 J. W. Jurss, J. J. Concepcion, J. M. Butler, K. M. Omberg, L. M. Baraldo, D. G. Thompson, E. L. Lebeau, B. Hornstein, J. R. Schoonover, H. Jude, J. D. Thompson, D. M. Dattelbaum, R. C. Rocha, J. L. Templeton and T. J. Meyer, *Inorg. Chem.*, 2012, **51**, 1345–1358.
4 W.-L. Ying, J. Emerson, M. J. Clarke and D. R. Sanadi, *Biochemistry*, 1991, **30**, 4949–4952.
5 J. Emerson, M. J. Clarke, W.-L. Ying and D. R. Sanadi, *J. Am. Chem. Soc.*, 1993, **115**, 11799–11805.
6 M. A. Matlib, Z. Zhou, S. Knight, S. Ahmed, K. M. Choi, J. Krause-Bauer, R. Phillips, R. Altschuld, Y. Katsube, N. Sperelakis and D. M. Bers, *J. Biol. Chem.*, 1998, **273**, 10223–10231.
7 S. R. Nathan, N. W. Pino, D. M. Arduino, F. Perocchi, S. N. MacMillan and J. J. Wilson, *Inorg. Chem.*, 2017, **56**, 3123–3126.
8 S. R. Nathan and J. J. Wilson, *J. Visualized Exp.*, 2017, DOI: 10.3791/56527.
9 M. J. Cleare and W. P. Griffith, *Chem. Commun.*, 1968, 1302.
10 M. J. Cleare and W. P. Griffith, *J. Chem. Soc. A*, 1970, 1117–1125.
11 W. P. Griffith and D. Pawson, *J. Chem. Soc., Dalton Trans.*, 1973, 1315–1320.
12 W. P. Griffith, N. T. McManus and A. C. Skapski, *J. Chem. Soc., Chem. Commun.*, 1984, 434–435.
13 W. P. Griffith, M. Jane Mockfrod and A. C. Skapski, *Inorg. Chim. Acta*, 1987, **126**, 179–186.
14 M. Haukka, T. Venäläinen, M. Ahlgrén and T. A. Pakkanen, *Inorg. Chem.*, 1995, **34**, 2931–2936.
15 M. Haukka, M. Ahlgrén and T. A. Pakkanen, *J. Chem. Soc., Dalton Trans.*, 1996, 1927–1933.
16 D. Sellman, T. Gottschalk-Gaudig and F. W. Heinemann, *Inorg. Chim. Acta*, 1998, **269**, 63–72.
17 T. Jüstel, J. Bendix, N. Metzler-Nolte, T. Weyhermüller, B. Nuber and K. Wieghardt, *Inorg. Chem.*, 1998, **37**, 35–43.
18 L. Bonomo, E. Solari, R. Scopelliti and C. Floriani, *Angew. Chem., Int. Ed.*, 2001, **40**, 2529–2531.

19 S. Matsumura, K. Shikano, T. Oi, N. Suzuki and H. Nagao, *Inorg. Chem.*, 2008, **47**, 9125–9127.
20 X.-Y. Yi, H.-Y. Ng, W.-M. Cheung, H. H. Y. Sung, I. D. Williams and W.-H. Leung, *Inorg. Chem.*, 2012, **51**, 10529–10535.
21 A. Glüer, B. Askevold, B. Schluschaß, F. W. Heinemann and S. Schneider, *Z. Anorg. Allg. Chem.*, 2015, **641**, 49–51.
22 H.-Y. Ng, W.-M. Cheung, E. Kwan Huang, K.-L. Wong, H. H.-Y. Sung, I. D. Williams and W.-H. Leung, *Dalton Trans.*, 2015, **44**, 18459–18468.
23 W.-M. Cheung, W.-H. Chiu, M. de Vere-Tucker, H. H.-Y. Sung, I. D. Williams and W.-H. Leung, *Inorg. Chem.*, 2017, **56**, 5680–5687.
24 M. Ciechanowicz and A. C. Skapski, *J. Chem. Soc. D*, 1969, 574–575.
25 M. Ciechanowicz and A. C. Skapski, *J. Chem. Soc. A*, 1971, 1792–1794.
26 R. J. D. Gee and H. M. Powell, *J. Chem. Soc. A*, 1971, 1795–1797.
27 D. De Stefani, R. Rizzuto and T. Pozzan, *Annu. Rev. Biochem.*, 2016, **85**, 161–192.
28 L. H. Opie, *Cardiovasc. Drugs Ther.*, 1991, **5**, 237–247.
29 G. C. Bompotis, S. Deftereos, C. Angelidis, E. Choidis, V. Panagopoulou, A. Kaoukis, V. P. Vassilikos, M. W. Cleman and G. Giannopoulos, *Med. Chem.*, 2016, **12**, 114–130.
30 G. de Jesús García-Rivas, A. Guerrero-Hernández, G. Guerrero-Serna, J. S. Rodríguez-Zavala and C. Zazueta, *FEBS J.*, 2005, **272**, 3477–3488.
31 G. de Jesús García-Rivas, K. Carvajal, F. Correa and C. Zazueta, *Br. J. Pharmacol.*, 2006, **149**, 829–837.
32 Y. Oropeza-Almazán, E. Vázquez-Garza, H. Chapoy-Villanueva, G. Torre-Amione and G. García-Rivas, *Oxid. Med. Cell. Longevity*, 2017, **2017**, 1–13.
33 K. J. Kamer and V. K. Mootha, *Nat. Rev. Mol. Cell Biol.*, 2015, **16**, 545–553.
34 P. M. Peixoto, L. M. Dejean and K. W. Kinnally, *Mitochondrion*, 2012, **12**, 14–23.
35 N. G. Connelly and W. E. Geiger, *Chem. Rev.*, 1996, **96**, 877–910.
36 V. V. Pavlishchuk and A. W. Addison, *Inorg. Chim. Acta*, 2000, **298**, 97–102.
37 *CrysAlisPro*, Rigaku OD, The Woodlands, TX, 2015.
38 G. M. Sheldrick, *Acta Crystallogr., Sect. C: Struct. Chem.*, 2015, **71**, 3–8.
39 G. M. Sheldrick, *Acta Crystallogr., Sect. A: Found. Crystallogr.*, 2008, **64**, 112–122.
40 P. Müller, *Crystallogr. Rev.*, 2009, **15**, 57–83.
41 O. V. Dolomanov, L. J. Bourhis, R. J. Gildea, J. A. K. Howard and H. Puschmann, *J. Appl. Crystallogr.*, 2009, **42**, 339–341.
42 A. N. Murphy, D. E. Bredesen, G. Cortopassi, E. Wang and G. Fiskum, *Proc. Natl. Acad. Sci. U. S. A.*, 1996, **93**, 9893–9898.
43 M. L. Good, M. D. Patil, L. M. Trefonas, J. Dodge, C. J. Alexander, R. J. Majeste and M. A. Cavanaugh, *J. Phys. Chem.*, 1984, **88**, 483–488.
44 P. C. Ford, D. P. Rudd, R. Gaunder and H. Taube, *J. Am. Chem. Soc.*, 1968, **90**, 1187–1194.
45 C. Cao, S. Wang, T. Cui, X.-C. Su and J. J. Chou, *Proc. Natl. Acad. Sci. U. S. A.*, 2017, **114**, E2846–E2851.